Characterizing excited-state intramolecular proton transfer in 3-hydroxyflavone and 3-hydroxy-2-(thiophen-2-yl)chromen-4-one with ultrafast transient infrared spectroscopy

Valerie S. Winkler[1] and Joseph A. Fournier[1*]

[1]Department of Chemistry, Washington University in St. Louis, St. Louis, MO, USA 63130

*corresponding author: jfournier@wustl.edu

Abstract

Vibrational dynamics associated with excited-state intramolecular proton transfer in 3-hydroxyflavone and 3-hydroxy-2-(thiophen-2-yl)chromen-4-one are characterized with ultrafast transient infrared spectroscopy. The spectroscopic data reveal rapid (<100 fs) proton transfer dynamics in both species, followed by vibrational relaxation of the tautomer products within a few picoseconds. Coherent coupling of the shared proton to low-frequency modes along the proton transfer coordinate is also observed.

Excited-state proton transfer reactions are a crucial class of reactions that are ubiquitous in biological systems, chemical catalysis, and photoredox chemistry.[1-2] Many model systems have been investigated to characterize the fundamental dynamics and mechanisms of proton transfer processes. In particular, 3-hydroxyflavone (3HF) is a prototypical system for the study of excited-state intramolecular proton transfer (ESIPT) reactions.[3-4] Upon UV excitation to the first electronic excited state (S_1), the "normal" enol isomer undergoes ESIPT to form the keto tautomer (referred to as the S_1' state), as depicted in Fig. 1. The S_0 to S_1 excitation is a $\pi\pi^*$ transition where significant electron density is removed from the enol OH group, resulting in a highly acidic proton where transfer to the tautomer S_1' structure becomes energetically favourable. Dual fluorescence from both the normal and tautomer states have been observed, with their ratio being highly dependent on solvent and temperature.[3-9] Due to ease of chemical modification of the 3HF scaffold, flavonoids and their derivatives have been widely explored as tuneable chemical probes and sensors.[10-14]

Time-resolved fluorescence and UV/Vis spectroscopic investigations of ESIPT in 3HF have reported an ultrafast proton transfer timescale of <100 fs in nonpolar solvents.[9,15-16] In polar solvents such as ethanol or acetonitrile, hydrogen bonding between the solvent and enol group disrupts the intramolecular hydrogen bond, resulting in a slower proton transfer timescale in the several picosecond regime.[17-18] Electronic spectroscopies, however, do not directly report on the nuclear motions driving the reaction dynamics. To this end, Chevalier et. al reported transient infrared spectra of 3HF in acetonitrile following UV excitation at 360 nm.[19] Global analysis of the transient vibrational spectra uncovered a 3.2 ps decay component assigned to the slower, solvent-inhibited ESIPT process. The 500 fs experimental resolution, however, did not allow the faster ESIPT component unperturbed by solvent to be measured.

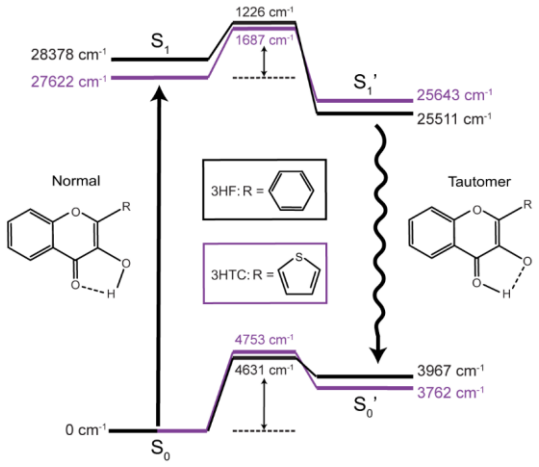

Fig. 1 Calculated energy level diagram for 3HF (black) and 3HTC (purple). Barrier heights relative to the S_0 and S_1 normal states are shown for the transition state levels. Calculations were performed at the B3LYP-D3BJ/aug-cc-pVDZ level of theory and basis set.

Numerous computational studies have also been performed on 3HF to investigate the ESIPT process.[20-24] These calculations predict a relatively small transfer barrier between the S_1 and S_1' states of approximately 700-1400 cm^{-1} (2-4 kcal/mol), suggesting a near-barrierless proton transfer reaction upon excitation into the Franck-Condon region.[24] Classical molecular dynamics simulations also predict an ultrafast (<100 fs) proton transfer component in gas phase or nonpolar solvents and slower picosecond components in polar solvents, in general agreement with experimental findings.

To better characterize ESIPT and provide improved experimental benchmarks for computational predictions, we have measured transient infrared spectra of 3HF and the derivative 3-hydroxy-2-(thiophen-2-yl)chromen-4-one (3HTC)[25] with approximately 100 fs resolution in a non-perturbing solvent (chloroform). Detailed experimental, computational, and data analysis methods are provided in the ESI.

The calculated (B3LYP-D3BJ/aug-cc-pVDZ) energy levels for isolated structures of the normal, transition state, and tautomer species in the ground and first excited electronic states for 3HF and 3HTC are shown in Fig. 1. Optimized structures for each species are given in Fig. S1. Small barriers between the normal and tautomer structures are predicted in the excited state, with 3HF calculated to have a barrier of about 1200 cm^{-1} and 3HTC about 1700 cm^{-1}, consistent with previous works.[18,26] Although the S_1 structure of 3HTC is lower in energy with respect to the ground-state compared to 3HF, the S_1' tautomer is higher in energy than that of 3HF. Consequently, the energy gap between the S_1 and S_1' minima is about 1000 cm^{-1} less in 3HTC compared to 3HF.

Transient infrared spectra following UV excitation are shown in Fig. 2a for 3HF (excitation wavelength 363 nm) and Fig. 2b for 3HTC (379 nm). The UV/Vis spectra of 3HF and 3HTC are provided in Fig. S2. In both species, there are two dominate ground-state bleach (negative) signals: the ketone carbonyl stretch near 1630 cm^{-1} and the enol OH bend near 1440 cm^{-1}. The positive signals correspond to vibrational transitions in the electronic excited state. In both species, the transient spectra show minor evolution after about 200 fs, indicating that the excited-state features beyond 200 fs derive from the S_1' tautomer and that ESIPT indeed occurs on a rapid timescale. The most intense excited-state features appear near 1300 and 1350 cm^{-1}, in reasonable agreement

with the two strongest calculated S_1' vibrational modes (blue stick spectra in Fig. 2) which are both predicted to have C-C and C-O stretch character (Fig. S3). Two weaker excited-state features appear near 1450 cm^{-1}, also in line with the calculated S_1' spectrum which predicts two transitions with CH and OH bend character. Transient IR spectra for 3HTC have not been previously reported, but show similar patterns to 3HF. An intense, closely spaced excited-state doublet feature appears near 1325 cm^{-1}. Based on the excited-state calculations, these features likely derive from normal modes with C-C stretch, C-O stretch, and CH bend character from the S_1' tautomer (Fig. S4). The other notable excited-state features at 1375 and 1450 cm^{-1} are consistent with predicted S_1' CH bend and OH bend transitions.

There are no unambiguous signatures, however, of the normal S_1 structure for either species. The strongest S_1 transitions (red stick spectra in Fig. 2) for both 3HF and 3HTC are predicted to fall near 1350 cm^{-1} and correspond to OH bending modes (Figs. S5 and S6). These transitions appear masked by the strong and broad S_1' background. More isolated vibrational features near 1275 cm^{-1} are also predicted in both species, again consisting of OH bend character. The transient spectra at 100 fs delay time does show larger intensity in this spectral region compared to later spectra, possibly indicating the presence of the S_1 species at the earliest delay times measured. The decay dynamics of the putative S_1 OH bend transitions near 1275 cm^{-1} are presented in Fig. 3. Sub-100 fs decay time constants were recovered for both 3HF (53 fs) and 3HTC (43 fs), providing a more direct experimental estimate for the ESIPT timescales. Despite

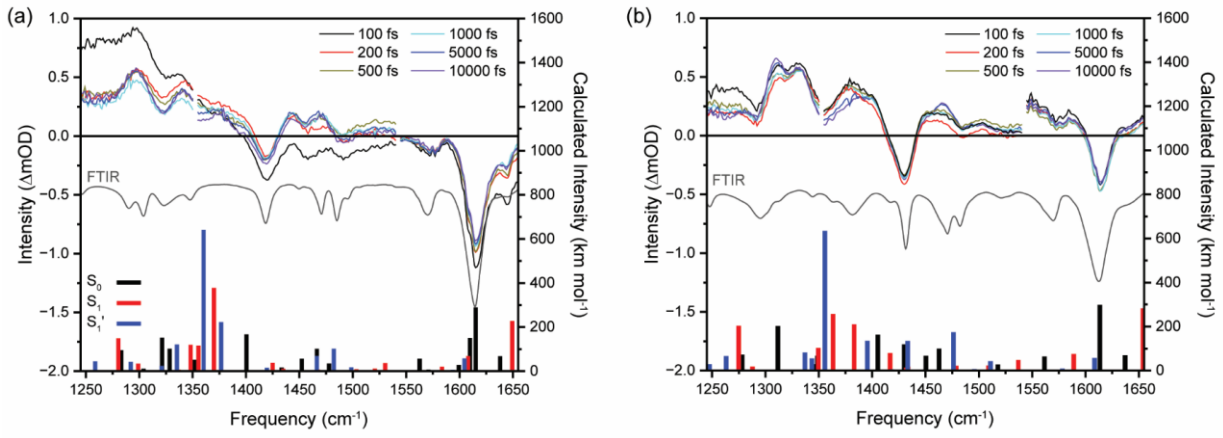

Fig. 2 Transient infrared spectra of (a) 3HF and (b) 3HTC at several selected delay times following UV excitation. FTIR spectra are presented as inverted grey traces in both panels. Calculated infrared spectra for optimized structures in the S_0 (black), S_1 (red), and S_1' (blue) states are displayed at the bottom of each panel (B3LYP-D3BJ/aug-cc-pVDZ, scaled by 0.975).

the differences in the energetic landscapes between 3HF and 3HTC (Fig. 1), the proton transfer timescales are equivalent within experimental uncertainty.

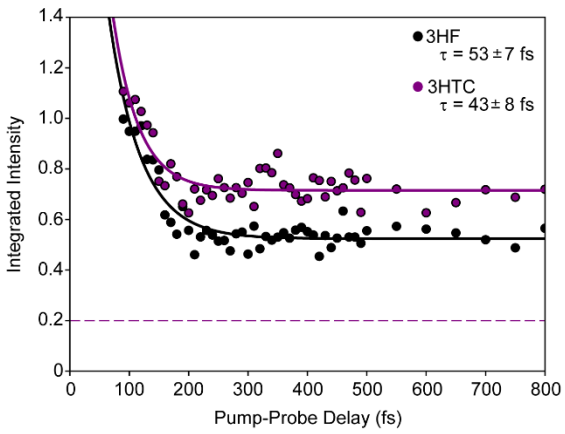

Fig. 3 Spectral decay dynamics of the lowest-energy S_1 OH bend transitions near 1275 cm^{-1} for 3HF (black dots) and 3HTC (purple dots). The data were fit to a monoexponential decay function, $f(t) = Ae^{-t/\tau} + b$ (solid lines). The exponential decay time constant, τ, and standard deviations are displayed inset and provide a measurement of the ESIPT timescale. The 3HTC data is offset by 0.2 (dashed purple line) for visual clarity.

The intramolecular H-bond in the ground S_0 state in both species is quite weak, with proton donor-acceptor distances between the sharing oxygen atoms of approximately 2.6 Å. This distance decreases significantly in the S_1 state, with optimized values close to 2.5 Å. The large decrease in the O-O distance suggests that strong anharmonic coupling exists between the proton degrees of freedom and low-frequency vibrational modes along the proton transfer coordinate. Interestingly, the OH bend ground-state transitions for 3HF and 3HTC exhibit oscillatory behaviour at early pump-probe delay times (Fig. 4). The presence of these oscillations is consistent with coherent coupling dynamics between the OH bend and low-frequency motion along the proton transfer coordinate within the ground-electronic S_0 state.[20, 24, 27-29] The oscillation periods of <300 fs in both species correspond to vibrational frequencies around 100 cm^{-1}. The calculations predict two modes in this low-frequency region that involve the proton donor and acceptor groups: an in-plane bending motion that bring the donor and acceptor oxygen atoms towards each other and an out-of-plane bending motion perpendicular to the proton transfer coordinate (Fig. S7). Both motions are likely to be important in the proton transfer process upon electronic excitation, where the in-plane mode would promote transfer while the out-of-plane mode would inhibit transfer. The measured proton transfer timescales, however, are much faster than the oscillation periods of these low-frequency modes involving the donor and acceptor groups. The rapid proton transfer timescales suggests that transfer could be driven mainly by high-frequency O-H motion instead of low-frequency heavy atom motions.[30] Coupling to higher-frequency heavy atom motions may also be present but cannot be resolved in the current experiments. Higher-order experiments that resolve the UV excitation axis (e.g., two-dimensional

electronic-vibrational spectroscopy) would be necessary to clearly discern vibrational wavepacket dynamics on the excited electronic surfaces.[31-32] It is also likely that nonadiabatic dynamics are at play, where proton transfer is correlated with the electronic coupling between the S_1 and S_1' electronic states.[33-35]

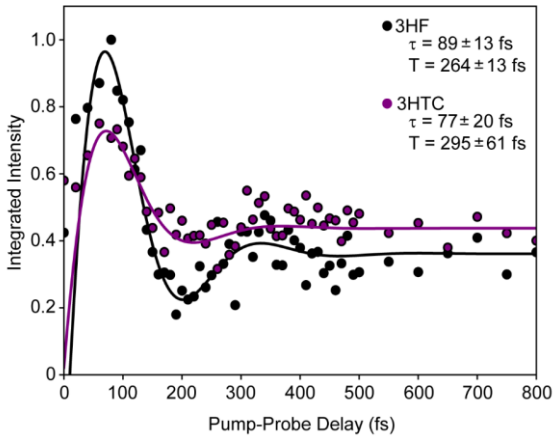

Fig. 4 Spectral dynamics of the S_0 ground-state OH bend transitions for 3HF (black dots) and 3HTC (purple dots). Fits to a damped oscillatory functions, $f(t) = A\sin\left(\frac{2\pi t}{T} + b\right)e^{-t/\tau} + c$, are given by solid lines. The exponential decay (τ) and oscillation period (T) fitting parameters and their standard deviations are shown inset. The oscillation periods are consistent with coupling between the shared proton's degrees of freedom and low-frequency motions along the proton transfer coordinate.

Global fit analysis of the transient spectra was next performed starting at 200 fs, following proton transfer. Two dominant decay associated spectral components were recovered for both 3HF and 3HTC, which are presented in Fig. 5. The largest component for each species, labelled A_0, is constant over the 10 ps experimental window and correspond to the ground-state bleach and the excited-state S_1' spectra. A weaker second profile observed for both compounds, labelled A_1, have monoexponential decay constants of about 1 ps for 3HF and 3 ps for 3HTC. Note that the frequency positions of the most intense features in both A_1 spectra match well with excited-state S_1' features in A_0. This observation suggests that the A_1 decay associated spectra correspond to changing intensities and frequencies of the S_1' state upon vibrational cooling following ESIPT. With 3HF and 3HTC having very similar structures, it is expected that intermolecular relaxation to the solvent will occur on similar timescales for both species. The timescale difference between 3HF and 3HTC, therefore, is more likely attributed to intramolecular relaxation processes. 3HF has nine more normal mode vibrations than 3HTC (78 vs. 69), offering more vibrational relaxation pathways following proton transfer. Alternatively, the larger energy gap between the S_1 and S_1' states in 3HF will result in greater initial vibrational energy in S_1' upon proton transfer. This higher initial vibrational energy in 3HF will yield faster vibrational relaxation compared to the less vibrationally hot S_1' state of 3HTC.

The observed rapid ESIPT dynamics and wavepacket dynamics on the ground state provide new experimental benchmarks for rapidly advancing theoretical methods. Approaches that treat the proton quantum mechanically, include nonadiabatic effects, and properly simulate vibrational energy flow using quantum dynamics will help unravel more detailed molecular-level mechanistic insight of ESIPT in 3HF and its derivatives. We posit that electronic excitation of 3HF and 3HTC leads to immediate delocalization of the shared proton wavefunction between the donor and acceptor groups, with rapid transfer occurring within a few periods of the O-H motion. Successful transfer is also likely incumbent upon strong coupling to relatively high-frequency heavy atom motions along the transfer coordinate. The vibrationally hot S_1' tautomer species then undergo vibrational relaxation in <5 ps. Improved fundamental understanding of ESIPT and vibrational relaxation mechanisms will aid in the development of more tuneable and sensitive molecular probes and sensors for material and biological applications.

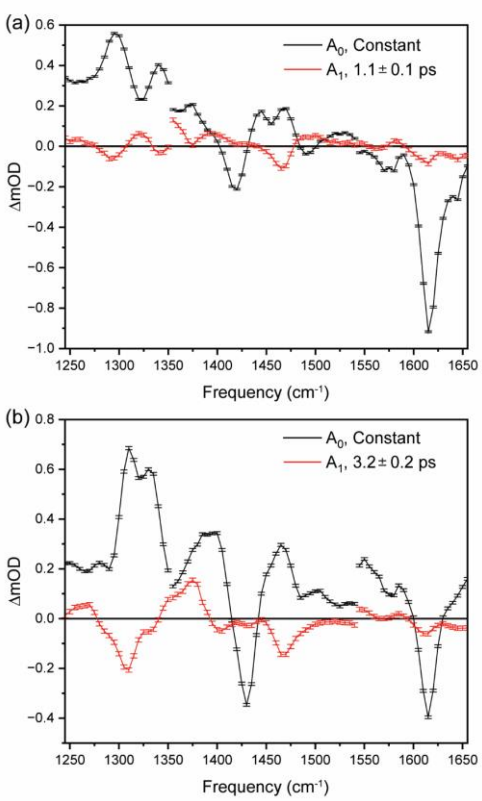

Fig. 5 Global fit analysis of the transient infrared spectra between 0.2-10 ps for (a) 3HF and (b) 3HTC. The A_0 components are static contributions representing the ground-state bleach and excited-state S_1' spectra. The A_1 components follow a monoexponential decay with time constants of about 1 ps and 3 ps for 3HF and 3HTC, respectively, and are assigned to vibrational cooling of the S_1' states following proton transfer.

Acknowledgments

This work was supported by the US National Science Foundation under grant CHE-2044927.

Conflicts of interest

There are no conflicts to declare.

Data availability

The following data are provided in ESI: Cartesian coordinates of the optimized S_0, S_1 and S_1' structures; transient infrared spectra at the pump-probe waiting times presented in Fig. 2.; data from the global fit analysis presented in Fig. 5. Data from all other pump-probe times are available on the Harvard Dataverse at https://doi.org/10.7910/DVN/Q7IQIH.

References

1 T. Kumpulainen, B. Lang, A. Rosspeintner and E. Vauthey, *Chem. Rev*., 2017, **117**, 10826–10939.

2 P. K. Sengupta and M. Kasha, *Chem. Phys. Lett*., 1979, **68**, 382.

3 G. J. Woolfe and P. J. Thistlethwaite, *J. Am. Chem. Soc*., 1981, **103**, 6919.

4 M. Itoh, K. Tokumura, Y. Tanimoto, Y. Okada, H. Takeuchi, K. Obi, and I. Tanaka. *J. Am. Chem. Soc*., 1982, **10**, 4146.

5 A. J. G. Strandjord, S. H. Courtney, D. M. Friedrich and P. F. Barbara, *J. Phys. Chem*., 1983, **87**, 1125-1133.

6 D. McMorrow and M. Kasha, *J. Phys. Chem*., 1984, **88**, 2235.

7 S. Protti and A. Mezzetti, *J. Mol. Liq*., 2015, **205**, 110–114.

8 S. Ameer-Beg, S. M. Ormson, R. G. Brown, P. Matousek, M. Towrie, E. T. J. Nibbering, P. Foggi and F. V. R. Neuwahl, *J. Phys. Chem. A*, 2001, **105**, 3709-3718.

9 M. Sarkar and P. K. Sengupta, *Chem. Phys. Lett*, 1991, **179**, 68.

10 A. Sytnik, D. Gormin and M. Kasha, *Proc. Natl. Acad. Sci. U.S.A.*, 1994, **91**, 11968−11972.

11 J. Guharay, B. Sengupta and P. K. Sengupta, *Proteins*, 2001, **43**, 75−81.

12 A. S. Klymchenko and A. P. Demchenko, *Langmuir*, 2002, **18**, 5637.

13 S. Chaudhuri, K. Basu, B. Sengupta, A. Banerjee and P. K. Sengupta, *Luminescence*, 2008, **23**, 397–403.

14 B. J. Schwartz, L. A. Peteanu and C. B. J Harris, *Phys. Chem*. 1992, **96**, 3591.

15 A. N. Bader, V. G. Pivovarenko, A. P. Demchenko, F. Ariese, and C. Gooijer, *J. Phys. Chem. B*, 2004, **108**, 10589.

16 T. C. Swinney and D. F. Kelley, *J. Phys. Chem*., 1991, **95**, 10369.

17 G. A. Brucker, T. C. Swinney and D. F. Kelley, *J. Phys. Chem.*, 1991, **95**, 3190.

18 K. Chevalier, M. M. N. Wolf, A. Funk, M. Andres, M. Gerhards and R. Diller, *Phys. Chem. Chem. Phys*., 2012, **14**, 15007–15020.

19 J. Stenger, D. Madsen, J. Dreyer, E. T. J. Nibbering, P. Hamm and T. Elsaesser, *J. Phys. Chem. A*, 2001, **105**, 2929–2932.

20 C. Chudoba, E. Riedle, M. Pfeiffer and T. Elsaesser, *Chem. Phys. Lett*., 1996, **263**, 622.

21 M. Balasubramanian, A. Reynolds, T. J. Blair and M. Khalil, *Chem. Phys.*, 2019, **519**, 38-44.

22 M. Nottoli, M. Bondanza, F. Lipparini and B. J. Mennucci, *Chem. Phys*., 2021, **154**, 184107.

23 Y. Li, F. Siddique, A. J. Aquino and H. Lischka, *J. Phys. Chem. A*, 2021, **125**, 5765-5778.

24 X. P. Chang, F. R. Fan, G. Zhao, X. Ma and T. S. Zhang, *Chem. Phys.*, 2023, **575**, 112056.

25 M. J. Colín, M. Á. Aguilar and M. E. Martín, *ACS Omega*, 2023, **8**, 19939-19949.

26 M. A. Bellucci and D. F. Coker, *J. Chem. Phys*., 2012, **136**, 194505.

27 D. Dziuba, I.A. Karpenko, N.P.F. Barthes, B. Y. Michel, A. S. Klymchenko, R. Benhida, A.P. Demchenko, Y. Mély and A. Burger, *Chem. Eur. J.*, 2014, **20**, 1998–2009.

28 H. Ma and J. Huang, *RSC Adv*., 2016, **6**, 96147.

29 L. Zhang, F. Fassioli, B. Fu, Z. S. She, and G. D. Scholes, *ACS Phys. Chem Au*, 2023, **3**, 107-118.

30 J. D. Gaynor and M. Khalil, *J. Chem. Phys.*, 2017, **147**, 094202.

31 J. D. Gaynor, J. Sandwisch, and M. Khalil, *Nat. Commun.*, 2019, **10**, 5621.

32 D. C. Borgis, S. Lee, and J. T. Hynes, *Chem. Phys. Lett.*, 1989, **162**, 19-26.

33 P. M. Kiefer and J. T. Hynes, *J. Phys. Chem. A*, 2004, **108**, 11793-11808.

34 A. Soudackov, E. Hatcher, and S. Hammes-Schiffer, *J. Chem. Phys.*, 2005, **122**, 014505.